analytical chemistry

ARTICLE

pubs.acs.org/ac

Amplified Detection of MicroRNA Based on Ruthenium Oxide Nanoparticle-Initiated Deposition of an Insulating Film

Yanfen Peng[†] and Zhiqiang Gao[*,†,‡]

[†]Institute of Bioengineering and Nanotechnology, 31 Biopolis Way, The Nanos, Singapore 138669

[‡]Department of Chemistry, National University of Singapore, 3 Science Drive 3, Singapore 117543

ABSTRACT: A highly sensitive microRNA (miRNA) biosensor that employs ruthenium oxide nanoparticle (RuO_2 NP)-initiated polymerization of 3,3′-dimethoxybenzidine (DB) and miRNA-templated deposition of an insulating poly(3,3′-dimethoxybenzidine) (PDB) film is described in this work. The biosensor was made of a mixed monolayer of oligonucleotide capture probes (CPs) and 4-mercaptoaniline on a gold electrode. Following hybridization with a RuO_2 NP-tagged target miRNA, a mixture of DB/H_2O_2 in pH 5.0 0.10 M acetate buffer was applied to the biosensor. The RuO_2 NPs serve as polymerization initiator/catalyst for the polymerization of DB. And the hybridized anionic miRNA strands and free CPs serve as templates, guiding the deposition of PDB. The amount of the deposited PDB and its insulating power directly correlated to the concentration of the target miRNA in solution. Electrochemical impedance spectroscopic tests showed that a linear charge-transfer resistance−concentration relationship from 6.0 fM to 2.0 pM was attained after 60 min of incubation in the DB/H_2O_2 mixture. There was no cross-hybridization between pre-miRNA and mature miRNA and very little cross-hybridization among closely related miRNA family members even at single-base-mismatched levels. This impedance-based biosensor offers an attractive alternative for miRNA expression profiling and may enable the development of a portable multiplexing miRNA profiling system.

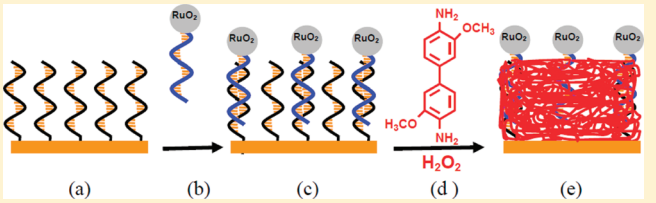

MicroRNAs (miRNAs) were discovered over 17 years ago through the pioneering work of Ambros and Ruvkun.[1,2] However, the study of miRNAs has grown exponentially only in the past few years. These RNAs are transcribed as long precursors and processed sequentially to hairpin pre-miRNAs, and then to mature miRNAs that are ∼22 nucleotides (nt) long with 3′-overhangs.[3,4] Up to date, 1048 miRNAs have been identified in the human genome.[5] MicroRNAs are believed to downregulate the expression of their target mRNAs (mRNAs) by base-pairing in the 3′ untranslated regions of their targets that either leads to mRNA degradation or translational repression, depending on the degree of complementary sequences between miRNAs and their targets.[6,7] It is believed that over one-third to one-half of all protein-encoding genes in humans are regulated by miRNAs.[8] Besides being recognized as key regulators in gene expression, accumulated studies have suggested that they also play important roles in a wide range of physiological and pathological processes, and cancer in particular.[9] Many examples have been found of miRNA aberrant expression in tumors, making them strong candidate oncogenes and tumor suppressors.[10−14] On the basis of several studies,[15−17] it has been suggested that miRNA expression profiling could be used for defining clinical phenotypes, as well as potentially useful molecular diagnostic markers.

As the number of identified miRNAs increases, microarrays appear to be an ideal platform for multiplex miRNA expression analysis since they offer the highest multiplexing capability and a wide dynamic range. Arrays containing tens of thousands of unique probe sequences can be constructed that enable simultaneous assessment of miRNAs expression associated with specific biological functions on a global scale. The short lengths of miRNAs with inherently different melting temperatures and the highly similar sequences between miRNA family members make probe design more difficult than for mRNA arrays. And the sensitivity and specificity of microarrays may somewhat be discounted as the risk of cross-hybridization is greatly increased.[18] The use of chemically modified nucleic acid probes like locked nucleic acid can elevate T_m and stabilize hybridization.[19] However, direct hybridization of miRNA samples onto the microarray requires a large amount of total RNA. When only a small and limited amount of RNA is available less abundant miRNAs may escape detection with the microarray technology.[19−21]

Fueled by the urgent need of a highly sensitive and reliable miRNA profiling tool, researchers turned their attention to quantitative real-time polymerase chain reaction (qRT-PCR) as it combines the exceptional amplification power of PCR with quantitative detection of the amplified products during each reaction cycle (real time). It offers the widest dynamic range, up to 8 orders of magnitude, while retaining most of the attractive features of PCR. However, the unique attributes of miRNAs mentioned earlier have also retarded the effectiveness of

Received: September 6, 2010
Accepted: December 14, 2010
Published: January 5, 2011

qRT-PCR because of the inability for much shorter primers to efficiently bind on such short miRNA templates.[20−22] To increase the specificity and efficiency of the PCR amplification step, miRNAs are first lengthened either by primer extension[23] or by using stem−looped primers,[24] generating extended sequences suitable for PCR amplification. Several qRT-PCR approaches for simultaneous amplification and quantification of miRNA have been developed recently.[23,24] Sensitivity and specificity were found to be dramatically improved. For example, the stem−loop qRT-PCR can profile miRNA expression with only nanograms of total RNA. More recently, a qRT-PCR-based array method became available which combined the high sensitivity provided by the stem−loop qRT-PCR with the ability to profile large numbers of miRNA in a single experiment. In comparison to a microarray of direct hybridization, qRT-PCR could be more prone to external variation as handling imperfection can also be amplified. The use of multiple references is generally accepted as the standard practice for qRT-PCR data normalization.

Despite the existence of microarray and miRNA qRT-PCR approaches, there is an increasing need for fast, reliable, and cost-effective assays, which are adaptable for any research settings interested in miRNA detection. It will offer an alternative for scientists interested in profiling miRNA expression in samples from different species and tissues. In addition, reliance on delicate optics and fragile enzymatic materials imposes a major hurdle to translate research-lab concepts to commercially viable products for point-of-care use. Because of the emerging diagnostic and prognostic values of miRNA, it is critical that the method for its expression profiling should be highly sensitive, specific, and only analyze mature miRNAs as they are the active form of miRNAs. The relatively limited number of miRNAs in humans, as compared to mRNAs,[5,25] offers excellent opportunity for electrical biosensors in miRNA expression profiling. Because of the inherent superiorities of electrical transduction methods, such as excellent compatibility with standard semiconductor technology, miniaturization, and low cost, electrical biosensors are able to provide high performance at low cost with a simple miniaturized readout and are exempt from the problems encountered in optical detection systems. Previously, we showed that electrical detection of subpicomolar miRNA could be achieved by using an interdigitated electrode array.[26] However, its sensitivity is not sufficiently high to permit PCR-free detection of miRNAs in clinically relevant samples without an RNA enrichment treatment. For example, to detect circulating miRNAs in blood without PCR, at least a femtomolar sensitivity is needed.[27] In this report, we present an electrochemical impedance-based biosensor along with a novel sensing protocol that enables amplified electrical detection of miRNA with significantly enhanced specificity and sensitivity. The biosensor was based on a direct ligation procedure that involves a chemical coupling reaction to directly tag miRNAs with ruthenium oxide nanoparticles (RuO_2 NPs). The RuO_2 NPs effectively catalyzed the polymerization of 3,3′-dimethoxybenzidine (DB), and the hybridized miRNA strands and free capture probe (CP) strands guided the deposition of poly(3,3′-dimethoxybenzidine) (PDB). The cumulative nature of the protocol greatly enhanced the sensitivity of the biosensor, lowering the detection limit to femtomolar levels. In practice, this biosensor meets the sensitivity and selectivity requirements for direct miRNA expression profiling, offering a promising alternative for miRNA research.

EXPERIMENTAL SECTION

Reagents. Thiolated oligonucleotide CPs used in this work were custom-made by Alpha-DNA (Montreal, Canada), and all other oligonucleotides of PCR purity were from First Base Pte Ltd. (Singapore). Total RNA extraction cocktail TRIzol reagent was from Invitrogen (Invitrogen, Carlsbad, CA). $Ru(NH_3)_6Cl_3$ (98%), $Ru(NH_3)_6Cl_2$ (99%), 4-(2-aminoethyl)pyridine (AEP), DB (99.5%), and 4-mercaptoaniline (MAn) (97%) were from Sigma-Aldrich (St. Louis, MO). $RuCl_3 \cdot xH_2O$ (∼40% Ru) was purchased from Merck (Darmstadt, Germany). All other reagents of certified analytical grade were obtained from Sigma-Aldrich and used without further purification. A pH 8.5 10 mM Tris−HCl−1.0 mM EDTA−0.10 M NaCl (TE) buffer solution was used as the hybridization and washing buffer. A pH 5.0 0.10 M acetate buffer containing 1.0 mM DB and 200 mM H_2O_2 was used as PDB deposition medium.

Apparatus. Electrochemical experiments were carried out using a CH Instruments model 660C electrochemical workstation (CH Instruments, Austin, TX). A conventional three-electrode system, consisting of a 2.0 mm diameter gold working electrode, a saturated calomel reference electrode (SCE), and a platinum foil counter electrode, was used in all electrochemical measurements. The electrochemical techniques used are cyclic voltammetry and electrochemical impedance spectroscopy (EIS). EIS experiments were conducted in 0.10 M sodium sulfate containing 5.0 mM of $Ru(NH_3)_6^{3+}/Ru(NH_3)_6^{2+}$ ($Ru(NH_3)_6^{3+/2+}$, 1/1) over a frequency range from 10 mHz to 100 000 Hz with a 5 mV sinusoidal voltage perturbation. $Ru(NH_3)_6^{3+/2+}$ in the sodium sulfate solution serve as redox probes so as to perform EIS. The potential of the electrochemical cell was offset to the formal potential of the redox probes. UV−vis spectra were recorded on a V-570 UV−vis spectrophotometer (Jasco Corp., Japan).

RuO_2 NP Synthesis, MicroRNA Extraction, and Tagging. The RuO_2 NPs with an average size of 3.0 nm were synthesized following a published procedure.[28] AEP coating was accomplished as follows: AEP, dissolved in water, was added to the nanoparticle suspension to a final concentration of 1.0 mM under stirring. After 60 min of stirring, 25 mL of ethanol was added and the mixture was centrifuged at 12 000 rpm. The RuO_2 NPs were then washed and centrifuged several times with 50% ethanol.

Total RNA was extracted using TRIzol reagent according to the manufacturer's recommended protocol. The yield and quality of total RNA were routinely assessed by gel electrophoresis and UV−vis spectrophotometry.[29] For example, the ratio of 28S rRNA/18S rRNA was found to be ∼2.0:1 with an average A260/A280 ratio of 1.99:1, indicating that high-quality and intact RNA was extracted from the samples.[29] The total RNA concentration was determined by UV−vis spectrophotometry. MicroRNAs in the total RNA were enriched by using a Montage spin column YM-50 (Millipore Corporation). RuO_2 NP tagging of miRNA was performed as follows: To 5.0 μg of total RNA solution was added 20 μL of 5 mM sodium periodate. The oxidation of the 3′ overhangs of miRNAs was carried out at 25 °C in the dark for 60 min. Then, 2-fold excess of sodium sulfite over sodium periodate was added to the reaction mixture followed by a 10 min incubation at 25 °C. Finally, 0.50 mg/mL of the RuO_2 NPs was added and the mixture was incubated at 37 °C for 3 h. The tagged miRNAs were collected and purified by two centrifugation−decantation−dispersion cycles with water and stored in a −20 °C freezer.

dx.doi.org/10.1021/ac102370s |Anal. Chem. 2011, 83, 820–827

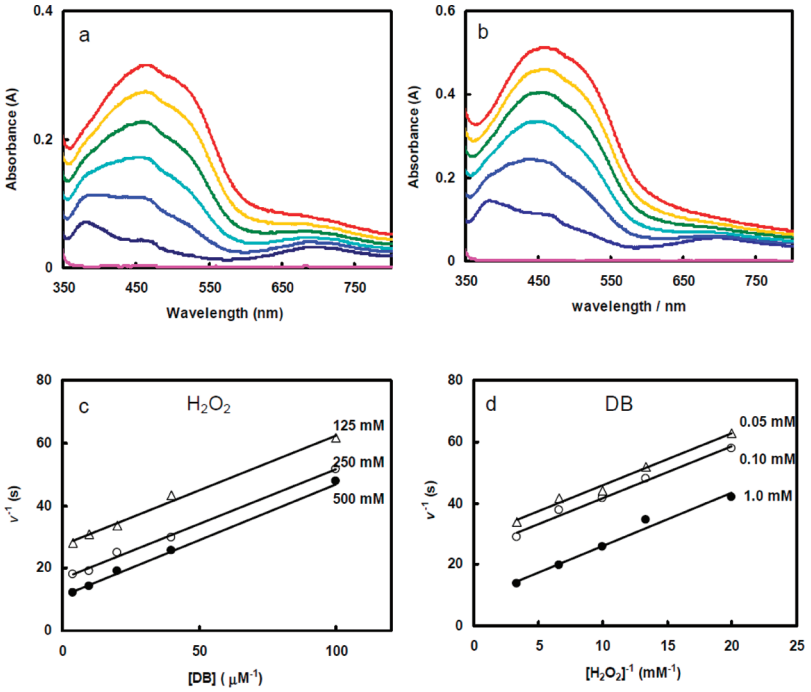

Figure 1. (a) UV−vis spectra of the oxidation of DB by H_2O_2 in the presence of HRP. The reaction mixture contained 0.5 mM DB, 10 mM H_2O_2, and 10 ng/mL HRP in pH 5.0 0.10 M acetate buffer. (b) UV−vis spectra of the oxidation of DB by H_2O_2 in the presence of RuO_2 NPs. The reaction mixture contained 1.0 mM DB, 200 mM H_2O_2, and 15 ng/mL RuO_2 NPs in pH 5.0 0.10 M acetate buffer. From bottom to top: 0, 30, 90, 150, 210, 270, and 330 s after the addition of HRP or RuO_2 NPs. (c and d) Double-reciprocal plots of the catalytic activity of RuO_2 NPs at a fixed concentration of one substrate vs varying concentration of the second substrate for H_2O_2 and DB.

Biosensor Preparation, Hybridization, and Detection. Before CP immobilization, a gold electrode was thoroughly polished with 0.05 μm alumina slurry and sonicated in water and ethanol for 5 min, respectively. Initial CP adsorption was accomplished by immersing the gold electrode in a phosphate-buffered saline (PBS) solution containing 100 μg/mL CP overnight at room temperature. The electrode was the copiously rinsed with PBS. To improve the quality and stability of the biosensor, the CP-coated electrode was immersed in 2.0 mg/mL MAn in ethanol for 2 h. During this treatment, MAn molecules fill in the defects via strong interaction between thiol and gold, forming a mixed monolayer with the CP. Excess MAn molecules were rinsed off, and the electrode was washed in stirred ethanol for 10 min, followed by a thorough rinsing with water.

The hybridization of the sample miRNA and its EIS detection were carried out as follows: First, the biosensor was placed in a moisture-saturated environmental chamber maintained at 10 °C below melting temperature. A 5.0 μL aliquot of hybridization solution containing the RuO_2 NP-tagged miRNA was uniformly spread onto the biosensor. It was rinsed thoroughly with a blank hybridization buffer at the hybridization temperature after 60 min. Finally, the biosensor was incubated in the DB/H_2O_2 mixture for 60 min. Electrochemical impedance of the biosensor was measured in the 0.10 M sodium sulfate containing 5.0 mM $Ru(NH_3)_6^{3+/2+}$. All potentials reported in this work were referred to the SCE, and all experiments were carried out at room temperature, unless otherwise stated.

RESULTS AND DISCUSSION

RuO_2 NP-Initiated Polymerization of DB. When a tiny amount of the RuO_2 NPs (<0.1 μg/mL) was spiked into the acetate buffer containing 1.0 mM DB and 200 mM H_2O_2, the mixture turned light blue in seconds, followed by a fast development of a yellow color accompanying the appearance of some brown precipitate (benzidine brown) after an extended period of reaction, mimicking that of peroxidase.[30,31] In accordance with horseradish peroxidase (HRP)-catalyzed oxidation and polymerization of DB (Figure 1a), the oxidation of DB by H_2O_2 in the presence of the RuO_2 NPs produced exactly the same colored products (Figure 1b). The first colored product is a blue charge-transfer complex of the parent diamine and diamine oxidation product with two adsorption maxima at ~380 and 680 nm.[31] Prolonged oxidation diminishes these two adsorption maxima, and there is an appearance of a new adsorption maximum at 470 nm, corresponding to the final yellow diimine.[30,31] The initial rate of oxidation varied linearly with the concentration of the RuO_2 NPs, suggesting that the oxidation of DB is first order with respect to the RuO_2 NPs. This is a good indication that the catalytic process may obey the Michaelis−Menten kinetics.[32] And more importantly, the linear dependence on the nanoparticle concentration strongly suggests that the RuO_2 NPs are homogeneously and stably dispersed in the reaction medium. To gain insight in the mechanism of the catalytic oxidation of DB in the presence of the RuO_2 NPs, a series of experiments were conducted over wide ranges of DB and H_2O_2 concentrations. It was found that the catalytic activity is pH-dependent, maximizing at pH 5.0. Parts c and d of Figure 1 show double-reciprocal plots of initial oxidation rate versus one substrate concentration, obtained at predetermined concentrations of the second substrate. The slopes of the lines are parallel, which is characteristic of a ping−pong mechanism,[33] indicating that, as for HRP, the RuO_2 NPs bind and react with the first substrate, releasing the first product before reacting with the second substrate. As an

dx.doi.org/10.1021/ac102370s |*Anal. Chem.* 2011, 83, 820–827

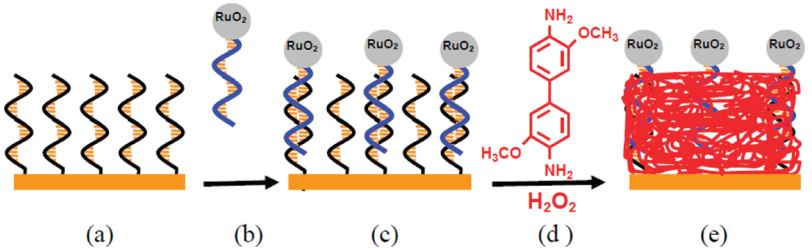

Figure 2. Schematic illustration of the miRNA biosensor based on RuO_2 NP-catalyzed miRNA-templated deposition of a thin PBD insulating film.

inorganic enzyme mimic, the RuO_2 NPs are expected to be more robust that their enzyme counterparts. Unlike natural peroxidase that can be easily deactivated in H_2O_2 solutions of high concentrations, at high temperatures, or at extreme pHs, it was found that the RuO_2 NPs remain active in a wide range of H_2O_2 concentration from micromolar to molar, a wide range of pH from 3 to 12, a wide range of temperature from 1 to 95 °C, and remain active after numerous cycles. In contrast, HRP does not show any appreciable activity after a treatment in H_2O_2 solutions at concentrations higher than 10 mM, pHs lower than 5, or temperatures higher than 50 °C. The robustness, in combination with high activity, small size, and good dispersion in aqueous media, makes the RuO_2 NPs ideal sensing materials for probing proteins and nucleic acids. As described below, an application of the RuO_2 NPs in the development of miRNA biosensors was investigated.

Detection Scheme. Figure 2 illustrates the workflow of the biosensor. A mixed monolayer of the thiolated CPs and MAn is self-assembled on the gold electrode, acting as a bioaffinitive interface (Figure 2a). The interactions of CPs with the RuO_2 NP-tagged target miRNAs (Figure 2b) via base-pairing form duplexes, bringing the RuO_2 NPs onto the biosensor surface (Figure 2c), the DB/H_2O_2 mixture is applied to the biosensor (Figure 2d). The hybridized anionic miRNA strands and free CPs serve as templates, the RuO_2 NPs as catalyst, for the polymerization of DB and the deposition of PDB (Figure 2e). The cumulative nature of the biosensor is particularly attractive, as high sensitivity is expected when the deposition of PDB is allowed to proceed for a sufficiently long period of time. The reason of using $Ru(NH_3)_6^{3+/2+}$ redox probes instead of other redox probes in the EIS experiments is twofold: to minimize unwanted changes in charge-transfer resistance, R_{ct}, and to have a low background R_{ct}. As we know, electrochemical reversibility, and hence R_{ct} of charged redox probes, is noticeably affected by electrostatic interaction with the polyanionic CP layer that the redox probes must penetrate to reach the electrode surface.[34,35] For example, the redox processes of $Fe(CN)_6^{3-/4-}$ become irreversible at oligonucleotide-coated electrodes even before hybridization, as evidenced by a drastically increased peak-to-peak potential separation (ΔE_p).[34−36] The increase in irreversibility for $Fe(CN)_6^{3-/4-}$ is due to repulsive electrostatic interaction impeding the ability of anionic $Fe(CN)_6^{3-/4-}$ to reach the electrode surface. As a direct consequence, significantly large values of R_{ct} are observed.[36] This large background R_{ct} precludes us from developing ultrasensitive miRNA biosensors. On the contrary, the cationic $Ru(NH_3)_6^{3+/2+}$ alleviate electrostatic repulsion between surface-immobilized CPs and the redox probes. No noticeable changes in the reversibility and R_{ct} of $Ru(NH_3)_6^{3+/2+}$ were observed among a bare gold electrode, a CP-coated gold electrode, and a hybridized biosensor before incubation, implying that $Ru(NH_3)_6^{3+/2+}$ is able to approach the electrode surface much more closely than $Fe(CN)_6^{3-/4-}$. In addition, as compared to other redox probes, such as $Fe(CN)_6^{3-/4-}$, the ultrafast electron-transfer rate of $Ru(NH_3)_6^{3+/2+}$ [37] produces an ultralow background R_{ct} and hence a high signal-to-noise ratio.

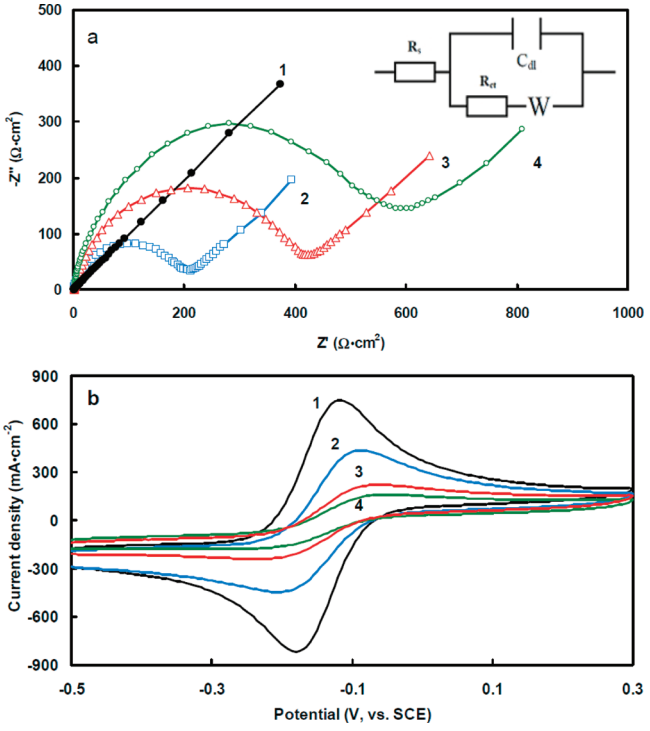

Figure 3. (a) EIS spectra and (b) the corresponding voltammograms at 100 mV/s of (1) control, (2) a biosensor hybridized to 50 ng total RNA, (3) curve 2 + 100 fM let-7c standard, and (4) curve 2 + 200 fM let-7c; 60 of min incubation in 1.0 mM DB/200 mM H_2O_2 in pH 5.0 0.10 M acetate buffer. EIS tests were conducted as described in the Experimental Section. Inset: Randle equivalent circuit; R_s, **solution resistance;** C_{dl}, **double layer capacitance;** R_{ct}, **charge-transfer resistance;** *W*, **Warburg impedance element.**

Feasibility Study. To test the feasibility of selectively detecting a specific miRNA by the biosensor in a rather complex matrix, 50 ng of total RNA was tested at a biosensor where CP was designed for let-7c. Presumably, upon hybridization, let-7c was selectively bound to its complementary CP and became fixed on the biosensor surface. A thin PDB insulating film was produced alongside the hybridized strands and free CP strands via the RuO_2 NP-initiated polymerization of DB, akin to that of HRP.[26,38] A typical EIS spectrum in the complex plane of the biosensor after the incubation in the DB/H_2O_2 mixture is shown in curve 2 in Figure 3a. The EIS spectrum consists of a semicircle at high frequencies followed by a straight line with a constant

dx.doi.org/10.1021/ac102370s |*Anal. Chem.* 2011, 83, 820–827

phase angle of 45°. This type of impedance spectrum is indicative of a thin-film-coated electrode system where the electron transfer is slow and the impedance is controlled by the interfacial charge transfer, manifesting itself by R_{ct} in the spectrum.[39] R_{ct} is the result of resistance to charge transfer between the redox probes and the biosensor through the deposited PDB film. The diameter of the semicircle is a measure of R_{ct}. It is the key parameter directly associated with the concentration of miRNA in the sample solution. Values of R_{ct} can be extracted from the EIS spectrum by fitting the spectrum to a Randle equivalent circuit (Figure 3a inset).[40] The straight line at low frequencies, on the other hand, represents the diffusion-controlled process in solution known as Warburg impedance (W).[40] For comparison, the EIS spectrum of a biosensor coated with noncomplementary CPs (control) after the same treatments is also given in Figure 3a. As seen in Figure 3a, a straight line was observed in the whole frequency range, suggesting that R_{ct} in this case is negligibly small, or the electron-transfer process is highly reversible and the electrode process is completely diffusion-controlled. Evidently, the significantly higher R_{ct} observed at the hybridized biosensor is a direct consequence of the hybridization and DB/H_2O_2 incubation, indicating that the formation of a thin PDB film on the biosensor effectively impedes electron transfer between the electrode and the redox probes. It is expected that the hybridization of the target miRNA to CP brings the RuO_2 NPs onto the biosensor surface. When the hybridized biosensor is incubated in the DB/H_2O_2 mixture, DB molecules are oxidized to cationic free radicals by H_2O_2 catalyzed by the RuO_2 NPs. And these free radicals are "collected" by the hybridized miRNA strands and the free CP strands through electrostatic interaction and chemical coupling.[41] This high cationic radical concentration around the miRNA and CP facilitates intramolecular coupling and hence spontaneous polymerization to form the insulating PDB film on the biosensor surface,[26,42] offering the much desired architecture for impedance sensing. The sizable increase in R_{ct} clearly indicated that an electron-insulating layer is formed on the biosensor surface as a result of hybridization and the incubation in the DB/H_2O_2 mixture, whereas in the control, no RuO_2 NPs were present on the biosensor surface since there was little hybridization between the noncomplementary CPs and miRNAs in the total RNA sample. A negligible increment in R_{ct} was observed, which is practically the same as those before the incubation in the DB/H_2O_2 mixture. These results clearly demonstrated that the biosensor selectively interacts with its target miRNA and the resulting CP/miRNA−RuO_2 NP adduct catalyzes the polymerization of DB and guides the deposition of PDB at the biosensor surface. The negligible increment in R_{ct} of the control also implies that nonhybridization-related uptake of miRNA is insignificant, facilitating the detection of miRNA at ultralow concentrations.

To further verify that the increase in R_{ct} is indeed due to the hybridized let-7c miRNA, successive aliquots of synthetic let-7c miRNA were spiked into the total RNA in 100 fM increments before RuO_2 tagging. As depicted by curves 3 and 4 in Figure 3a, further increases in R_{ct} were observed. Furthermore, the increase in R_{ct} observed for the spiked-in total RNA correlated linearly with the increase in let-7c miRNA concentration, while R_{ct} remained unchanged when 10 pM let-7c pre-miRNA was spiked into the total RNA instead of the mature let-7c miRNA, suggesting that the increase in R_{ct} generated in the total RNA sample is genuinely originated form let-7c and giving a preliminary indication of the specificity of the biosensor.

Figure 3b shows the corresponding cyclic voltammograms of the control and the biosensor of Figure 3a in the $Ru(NH_3)_6^{3+/2+}$ solution. As seen in Figure 3b, the voltammogram for the $Ru(NH_3)_6^{3+/2+}$ at the control showed the reduction and oxidation peaks that are typical for a reversible one-electron process. Practically identical voltammograms were obtained at the bare gold electrode, the CP-coated gold electrode, and the hybridized biosensor before the DB/H_2O_2 incubation. The voltammogram of the hybridized biosensor after the DB/H_2O_2 incubation exhibited a much reduced signal (~50% of that of the bare gold electrode) because of the $Ru(NH_3)_6^{3+/2+}$ redox probes in what can now be described as a quasireversible system with a large ΔE_p of ~120 mV, as the electronic communication between the redox probes and the gold electrode is effectively blocked by the deposited PDB film. Electron transfer between the redox probes and the gold electrode has to go though the thin PDB film. This dramatic increase in distance between the gold electrode and the redox probes will result in a slower electron-transfer rate, which in voltammogram is reflected by an increase in ΔE_p. On the basis of the small faradaic current produced from the redox probes, the PDB film appears to be tightly packed, resulting in excellent insulation of the substrate gold electrode. In addition, the electrostatic repulsion between the PDB film on the electrode surface and the cationic $Ru(NH_3)_6^{3+/2+}$ redox probes has to be considered, which does not allow for an effective penetration of the PDB layer by the positively charged redox probes. Nevertheless, the resulting PDB layer does not completely block the redox activity of $Ru(NH_3)_6^{3+/2+}$. We believe that the electron passes through defective sites rather than through the PDB layer. Consistent with the EIS data, further increase in ΔE_p and decrease in the faradaic current were observed when aliquots of let-7c standard were spiked into the total RNA sample.

Optimization. The above results confirmed that let-7c is successfully detected from the RNA mixture with high specificity. However, for a successful adaptation of the proposed strategy in ultrasensitive miRNA assay, the analytical signal must be exclusively associated with the concentration of the analyzed miRNA in a straightforward manner. In the case of PDB deposition, the deposition rate must be determined by one of the following: (i) mass-transport process of DB in solution and (ii) RuO_2 NP-catalyzed polymerization at the biosensor−solution interface. Under well-controlled conditions, when the mass transport is much faster than the polymerization, the deposition rate is then solely controlled by the polymerization process, which is in turn, controlled by the total amount of hybridized miRNA (RuO_2 NPs) at the biosensor surface. This sole RuO_2 NP-controlled process can be achieved by "speeding up" mass transport as the mass-transport rate is directly proportional to the concentration of the substrate. Higher mass-transport rates are easily attainable when working with higher concentrations of DB and H_2O_2. As DB concentration was increased, R_{ct} rose rapidly and almost linearly at first, but then slowed until maximal R_{ct} was reached (Figure 4a). It was observed that R_{ct} is practically independent of DB concentration at ≥1.0 mM, suggesting that the RuO_2 NP amplification does not appreciably deplete the concentration of DB. The PDB deposition rate is now solely determined by the amount of RuO_2 NPs brought to the biosensor surface. Similarly, the sensitivity increased with increasing H_2O_2 concentration and a maximum was attained at 200 mM H_2O_2 (Figure 4b). Figure 4c depicts the dependence of R_{ct} on solution pH. The pH of the deposition solution was adjusted by adding a 0.10 M NaOH or a 0.10 M H_2SO_4. It was observed that the pH of the PDB

dx.doi.org/10.1021/ac102370s |Anal. Chem. 2011, 83, 820–827

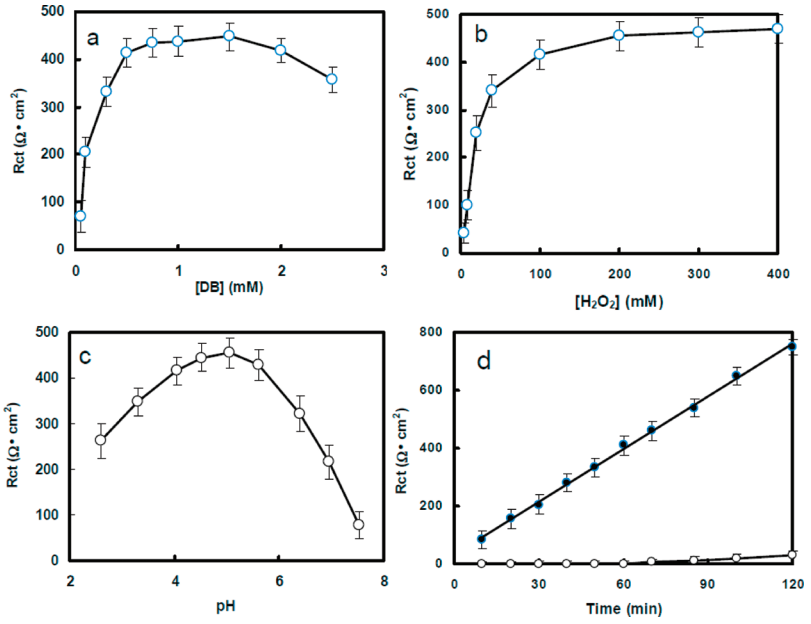

Figure 4. Dependence of R_{ct} on (a) DB, (b) H_2O_2, (c) pH, and (d) deposition time; 200 fM let-7c, other conditions are as for Figure 3.

deposition medium has a profound effect on R_{ct} of the biosensor. As illustrated in Figure 4c, when the pH value was changed from 7.0 to 5.0, R_{ct} increased sharply, presumably due to the increase in RuO_2 NP stability and activity. The highest sensitivity was attained at pH 5.0. Further increase in acidity did not result in an appreciable increase in R_{ct}, owing largely to the maximized catalytic activity of the RuO_2 NPs at pH 5.0.

To leverage on the cumulative nature of the process for further sensitivity improvement, a series of EIS tests were conducted. A plot of R_{ct} at different incubation times is shown in Figure 4d. In all cases, an immediate increase in R_{ct} was observed due to the deposition of PDB. Interestingly, the sensitivity of the biosensor was proportional to the incubation time throughout, indicating that there is very little activity loss of the RuO_2 NPs during incubation. To speed up the assay while keeping a reasonably high sensitivity, it was found that 60 min of incubation is sufficient to detect miRNA at femtomolar levels. After a much longer deposition time, R_{ct} of the control (background signal) became noticeable probably due to nonspecific deposition of PDB. For example, the background R_{ct} increased significantly from 0.5 $\Omega \cdot cm^2$ after 60 min of incubation to ~27 $\Omega \cdot cm^2$ after 120 min of incubation, deteriorating the detection limit from femtomolar to subpicomolar levels. Therefore, the incubation time of 60 min was chosen to ensure sufficiently high sensitivity and good signal-to-noise ratios.

Analytical Characteristics. The selectivity of the biosensor was evaluated by analyzing members in the let-7 family with the biosensor coated with CPs only complementary to let-7c. There is only one nucleotide difference out of 22 nucleotides between let-7c and let-7a and b, implying that the biosensor for let-7c is one-base-mismatched for let-7a and b. As shown in Figure 5, R_{ct} dropped by ~93% (selectivity factor of 14) to as low as 29 $\Omega \cdot cm^2$ when let-7a and b were tested on the biosensor. And selectivity factors of 26 and >200 against let-7e and f (two-base-mismatched miRNAs) and let-7d and g (three-base-mismatched miRNAs) were observed, respectively. And no R_{ct} changes over the control were detected when the let-7c biosensor was tested against let-7i (four-base-mismatched miRNAs). This selectivity

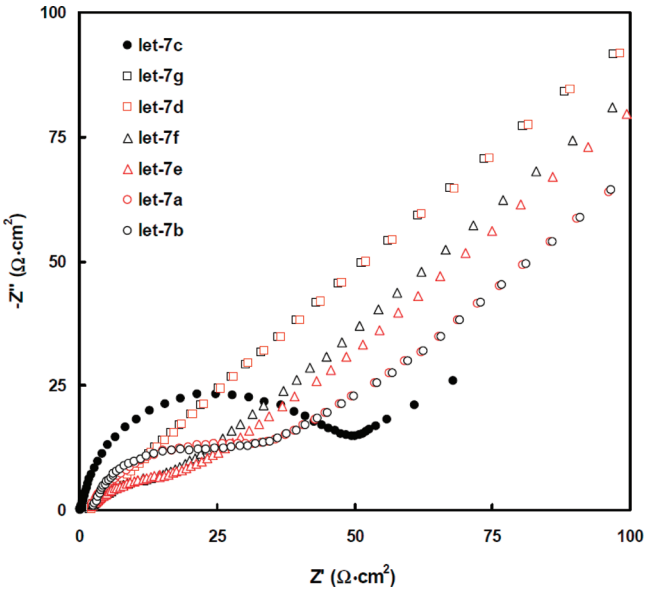

Figure 5. EIS responses of a let-7c biosensor to the members of the let-7 family. Conditions are as in Figure 3. For comparison, the spectrum of let-7c was scaled down 10 times.

between perfectly complementary and mismatched sequences of this biosensor is much better than those previously reported in other electrochemical DNA sensors,[28,29,43] probably due to the beneficial effect of the nanoparticulate tag on the hybridization selectivity.[44,45] The mismatch tests agreed well with the EIS results and confirmed that miRNA was successfully detected with high specificity and sensitivity.

Three mature miRNAs, miR-720 (17 nt), let-7c (22 nt), and miR-1248 (27 nt), ranging from the shortest (17 nt) to the longest (27 nt) miRNAs, were used as calibration standards to test the performance of the biosensor. The 60 min incubation in the DB/H_2O_2 mixture generated a dynamic range of 6.0 fM to 2.0 pM with a relative standard derivation of <12% at 200 fM and

dx.doi.org/10.1021/ac102370s |*Anal. Chem.* 2011, 83, 820–827

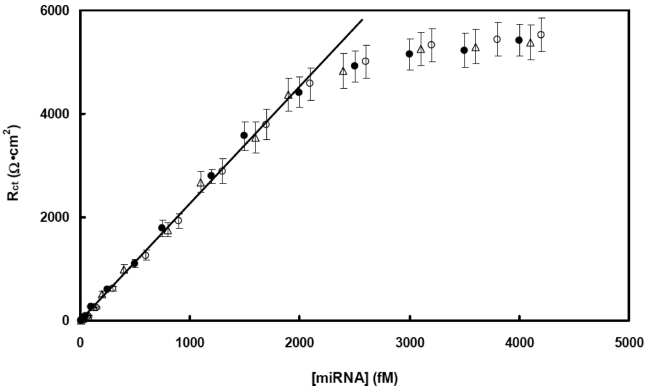

Figure 6. Calibration curves for (△) miR-720, (●) let-7c, and (○) miR-1248. Conditions are as for Figure 3.

Table 1. Analysis of miRNA in Total RNA Extracted from Cell Lines

	let-7a (10^6 copies/ μg of RNA)	let-7b (10^6 copies/ μg of RNA)	let-7c (10^6 copies/ μg of RNA)
HeLa cells	8.6 ± 1.3	21 ± 2.3	6.6 ± 0.82
	(8.2 ± 1.0)[a]	(23 ± 2.1)	(7.4 ± 0.79)
lung cancer cells	2.0 ± 0.19	2.5 ± 0.32	2.3 ± 0.24
	(2.2 ± 0.18)	(2.7 ± 0.35)	(2.1 ± 0.23)
normal cells	4.7 ± 0.66	8.3 ± 0.93	7.0 ± 0.87
	(4.5 ± 0.39)	(8.6 ± 0.88)	(6.3 ± 0.74)

[a] Data in parentheses were obtained by qRT-PCR.

a detection limit of ~3.0 fM at a signal-to-noise ratio of 3.0 (Figure 6). This catalyst and template dual-dependence of signal amplification substantially suppresses nonhybridization-related background noise since neither nonspecifically adsorbed miRNA strands nor RuO_2 NPs alone are able to initiate the deposition of PDB.

MicroRNA Expression Analysis. With the much improved sensitivity, the biosensor allowed us to directly and PCR-freely analyze miRNA expression in total RNA extracted from cell lines. Expression levels of three representative miRNAs in the let-7 family were determined by the biosensor and by qRT-PCR. As listed in Table 1, the results obtained with the biosensor are in good agreement with those obtained by qRT-PCR on the same sample and consistent with recently published data of miRNA expression profiling.[46,47] The lowest amount of total RNA needed for successful miRNA detection was found to be <3.0 ng, corresponding to <100 cells.[48] The relative errors associated with miRNA assays on individual miRNAs were generally less than 15% in the concentration range of 20 fM to 2.0 pM. This biosensor offers a greater accuracy in the identification of differentially expressed miRNAs and cuts down on the amount of total RNA and the need for running too many replicates.

CONCLUSION

In summary, we demonstrated in this report the utility of a nanoparticulate enzyme mimic in the development of ultrasensitive miRNA biosensors. The association of the nanoparticulate enzyme mimic to miRNA leads to the formation of a catalytic system on the biosensor surface that catalyzes the polymerization of DB and guides the deposition of PDB upon adding the DB/H_2O_2 mixture. Although the concept of engaging amplification by polymerization and an integral factor to enhance the sensitivity of the biosensor has been illustrated using only three miRNAs, it could easily be extended to a wide range of miRNAs of clinical, biological, and environmental significance. This biosensor is also easily extendable to a low-density array of 50−100 sensing nodes. The relatively limited number of miRNAs offers an excellent opportunity for the low- to medium-density electrical sensor array in miRNA expression profiling. In addition, the miRNA-guided deposition of PDB combined with efficient catalysis offers an attractive means to amplify the signal of hybridization-based miRNA biosensors. It could be adopted by a range of other detection techniques and mass-sensitive techniques in particular, such as quartz-crystal microbalance and surface plasmon resonance for sensitivity enhancement, greatly facilitating the development of a simple, low-cost, and portable detection system for point-of-care and field uses. On the other hand, the direct tagging and chemically amplified detection substantially prolonged the assay time. To be an attractive alternative for miRNA expression profiling, the unpopularity of impedance-based nucleic acid sensors is another hurdle to be overcome. The eventual acceptance of impedance-based biosensors for diagnostic applications will depend on how these novel schemes compare with the widely accepted technologies, i.e., microarray and qRT-PCR, in terms of simplicity, sensitivity, specificity, and reliability.

AUTHOR INFORMATION

Corresponding Author

*E-mail: zqgao@ibn.a-star.edu.sg or chmgz@nus.edu.sg. Phone: 6824-7113. Fax: 6478-9085.

ACKNOWLEDGMENT

This research is funded by the Agency for Science, Technology and Research through the Institute of Bioengineering and Nanotechnology, Republic of Singapore.

REFERENCES

(1) Wightman, B.; Ha, I.; Ruvkun, G. *Cell* **1993**, *75*, 855–862.
(2) Lee, R. C.; Feinbaum, R. L.; Ambros, V. *Cell* **1993**, *75*, 843–854.
(3) Hutvagner, G.; Zamore, P. D. *Science* **2001**, *293*, 834–838.
(4) Lee, Y.; Ahn, C.; Han, J.; Choi, H.; Kim, J.; Yim, J.; Lee, J.; Provost, P.; Radmark, O.; Kim, S. *Nature* **2003**, *425*, 415–419.
(5) miRBase: the microRNA Database. http://www.mirbase.org, release 16.0; September 2010; accessed: December 30, 2010.
(6) Bartel, D. P. *Cell* **2004**, *116*, 281–297.
(7) Engels, B. M.; Hutvagner, G. *Oncogene* **2006**, *25*, 6163–6169.
(8) Lewis, B. P.; Burge, C. B.; Bartel, D. P. *Cell* **2005**, *120*, 15–20.
(9) Stefani, G.; Slack, F. J. *Nat. Rev. Mol. Cell Biol.* **2008**, *9*, 219–230.
(10) Calin, G. A.; Croce, C. M. *Nat. Rev. Cancer* **2006**, *6*, 857–866.
(11) Esquela-Kerscher, A.; Slack, F. J. *Nat. Rev. Cancer* **2006**, *6*, 259–269.
(12) Zhang, B. H.; Cobb, G. P.; Anderson, T. A. *Dev. Biol.* **2007**, *302*, 1–12.
(13) Croce, C. M.; Calin, G. A. *Cell* **2005**, *122*, 6–7.
(14) Lu, J.; Getz, G.; Miska, E. A.; Alvarez-Saavedra, E.; Lamb, J.; Peck, D.; Sweet-Corderob, A.; Ebert, B. L.; Mak, R. H.; Ferrando, A. A.; Downing, J. R.; Jacks, T.; Horvitz, H. R.; Golub, T. R. *Nature* **2005**, *435*, 834–838.
(15) Hammond, S. M. *Curr. Opin. Genet. Dev.* **2006**, *16*, 4–9.

(16) Nam, E. J.; Yoon, H.; Kim., S. W. *Clin. Cancer Res.* **2008**, *14*, 2690–2695.
(17) He, L.; Thomson, J. M.; Hemann, M. T.; Hernando-Monge, E.; David Mu, D.; Goodson, S.; Powers, S.; Cordon-Cardo, C.; Lowe, S. W.; Hannon, G. J.; Hammond, S. M. *Nature* **2005**, *435*, 828–833.
(18) Li, W.; Ruan, K. C. *Anal. Bioanal. Chem.* **2009**, *394*, 1117–1124.
(19) Castoldi, M.; Schmidt, S.; Benes, V.; Hentze, M. W.; Muckenthaler, M. U. *Nat. Protoc.* **2008**, *3*, 321–329.
(20) Liu, C.-G.; Calin, G. A.; Meloon, B.; Gamliel, N.; Sevignani, C.; Ferracin, M.; Dumitru, C. D.; Shimizu, M.; Zupo, S.; Dono, M. *Proc. Natl. Acad. Sci. U.S.A.* **2004**, *101*, 9740–9744.
(21) Krichevsky, A. M.; King, K. S.; Donahue, C. P.; Khrapko, K.; Kosik, K. S. *RNA* **2003**, *9*, 1274–1281.
(22) Calin, G. A.; Liu, C. G.; Sevignani, C.; Ferracin, M.; Felli, N.; Dumitru, C. D.; Shimizu, M.; Cimmino, A.; Zupo, S.; Dono, M. *Proc. Natl. Acad. Sci. U.S.A.* **2004**, *101*, 11755–11760.
(23) Raymond, C. K.; Roberts, B. S.; Garrett-Engele, P.; Lim, L. P.; Johnson, J. M. *RNA* **2005**, *11*, 1737–1744.
(24) Chen, C. F.; Ridzon, D. A.; Broomer, A. J.; Zhou, Z.; Lee, D. H.; Nguyen, J. T.; Barbisin, M.; Xu, N. L.; Mahuvakar, V. R.; Andersen, M. R.; Lao, K. Q.; Livak, K. J.; Guegler, K. J. *Nucleic Acids Res.* **2005**, *33*, e179.
(25) Berezikov, E.; Guryev, V.; van de Belt, J.; Wienholds, E.; Plasterk, R. H.; Cuppen, E. *Cell* **2005**, *120*, 21–24.
(26) Fan, Y.; Chen, C. T.; Tung, C.; Kong, J. M.; Gao, Z. Q. *J. Am. Chem. Soc.* **2007**, *129*, 5437–5443.
(27) Mitchell, P. S.; Parkin, R. K.; Kroh, E. M.; Fritz, B. R.; Wyman, S. K.; Pogosova-Agadjanyan, E. L.; Peterson, A.; Noteboom, J.; O'Briant, K. C.; Allen, A.; Lin, D. W.; Urban, N.; Drescher, C. W.; Knudsen, B. S.; Stirewalt, D. L.; Gentleman, R.; Vessella, R. L.; Nelson, P. S.; Martin, D. B.; Tewari, M. *Proc. Natl. Acad. Sci. U.S.A.* **2008**, *105*, 10513–10518.
(28) Rossi, L. M.; Dupont, J.; Machado, G.; Fichtner, P. F. P.; Radtke, C.; Baumvol, I. J. R.; Teixeire, R. *J. Chem. Soc.* **2004**, *15*, 904–910.
(29) Sambrook, J.; Fritsch, E. F.; Maniatis, T. *Molecular Cloning, A Laboratory Manual*, 2nd ed.; Cold Spring Harbor Laboratory Press: Cold Spring Harbor, NY, 1989.
(30) Li, P.; Gao, Z.; Xu, Y.; Zhao, Z. *Anal. Chim. Acta* **1990**, *229*, 213–219.
(31) Claiborne, A.; Fridovich, I. *Biochemistry* **1979**, *18*, 2325–2329.
(32) Michaelis, L.; Menten, M. L. *Biochem. Z.* **1913**, *49*, 333–369.
(33) Porter, D. J. T.; Bright, J. H. *J. Biol. Chem.* **1982**, *258*, 9913–9924.
(34) Tansil, N. C.; Xie, H.; Xie., F. *Anal. Chem.* **2005**, *77*, 126–134.
(35) Xie, H.; Zhang, C.; Gao, Z. Q. *Anal. Chem.* **2004**, *76*, 1611–1617.
(36) Long, Y. T.; Li, C. Z.; Sutherland, C. T.; Kraatz, H. B.; Lee, J. S. *Anal. Chem.* **2004**, *76*, 4059–4065.
(37) Meyer, T. J.; Taube, H. *Inorg. Chem.* **1968**, *7*, 2369–2372.
(38) Su, X. D.; Teh, H. F.; Aunga, K. M. M.; Zonga, Y.; Gao, Z. Q. *Biosens. Bioelectron.* **2008**, *23*, 1715–1720.
(39) Gao, Z. Q.; Ivaska, A.; Zha, T. *Talanta* **1993**, *40*, 399.
(40) Randles, J. E. B. *Discuss. Faraday Soc.* **1947**, *1*, 11–13.
(41) Fourney, R. M.; O'Brien, P. J.; Davidson, W. S. *Carcinogenesis* **1986**, *7*, 1535–1542.
(42) Nagarajan, R.; Liu, W.; Kumar, J.; Tripathy, S. K.; Brono, F. F.; Samuelson, L. A. *Macromolecules* **2001**, *34*, 3921–3927.
(43) Gao, Z. Q.; Yang, Y. C. *Anal. Chem.* **2006**, *78*, 1470–1477.
(44) Storhoff, J. J.; Elghanian, R.; Mucic, R. C.; Mirkin, C. A.; Letsinger, L. R. *J. Am. Chem. Soc.* **1998**, *120*, 1959–1964.
(45) Elghanian, R.; Storhoff, J. J.; Mucic, R. C.; Letsinger, R. L.; Mirkin, C. A. *Science* **1997**, *277*, 1078–1081.
(46) Nelson, P. T.; Baldwin, D. A.; Scearce, L. M.; Oberholtzer, J. C.; Tobias, J. W.; Mourelatos, Z. *Nat. Methods* **2004**, *2*, 155–161.
(47) Allawi, H. T.; Dahlberg, J. E.; Olson, S.; Lund, E.; Olson, M.; Ma, W. P.; Takova, T.; Neri, B. P.; Lyamichev, V. I. *RNA* **2004**, *10*, 1153–1161.
(48) Lim, L. P.; Lau, N. C.; Weinstein, E. G.; Abdelhakim, A.; Yekta, S.; Roades, M.; Burge, C. B.; Bartel, D. P. *Genes Dev.* **2003**, *17*, 991–1008.